scientific reports

Check for updates

OPEN

Rosmarinic acid alleviates bleomycin-induced pulmonary fibrosis in mice by activating the Rap1 pathway

Aman Gul[1,2,3,4,7], Yuanyuan Zhong[2,3,5,7], Maimaiti Aili[1], Cong Xie[2,3], Ainiwaer Talifu[1,6], Shixia Huo[1], Yilifanjiang Kuerban[1], Maimaititusun Yalkun[2,3], Zhi Jian Li[1]✉ & Jingcheng Dong[2,3]✉

The efficiency of rosmarinic acid (RA) in treating bleomycin (BLM)-induced pulmonary fibrosis (PF) was reported, but mechanisms are unclear. RA, from *Herba japonica*, is used for air-inflammatory and fibrotic diseases like PF. Its anti-inflammatory and anti-fibrotic roles remain unclear. The study evaluated RA's effectiveness in treating PF and clarified therapeutic mechanisms. A mouse PF model was established with 5U/kg BLM. RA was given daily from Day 3 for 25 days at 20, 40, or 80 mg/kg. Pirfenidone (PFD) at 300 mg/kg was the positive control. RA's efficacy was assessed using lung PET-CT and evaluations of pulmonary inflammation, function, and fibrosis. And 4D label-free quantitative proteomics analysis was used to explore mechanisms, corroborated by Western blotting, and immunohistochemistry. RA at 40 mg/kg showed comparable efficacy to PFD and was more effective than 20 mg/kg and 80 mg/kg doses in treating BLM-induced PF in mice. Proteomics and KEGG analysis indicated treatment of RA partially restored protein expression and activated the RAP1 signaling pathway, upregulating proteins like FGF1, Kit, Kras, and Src. RA significantly alleviates BLM-induced PF in mice, with the best results at 40 mg/kg, due to RAP1 pathway activation.

Keywords PF, Rosmarinic acid, Bleomycin, RAP1 signaling pathway, 4D label-free quantitative proteomics

Abbreviations

RA	Rosmarinic acid
BLM	Bleomycin
PF	Pulmonary fibrosis
PFD	Pirfenidone
IHC	Immunohistochemistry

Pulmonary fibrosis is a chronic progressive disorder of unknown etiology, characterized by patchy scarring and a poor prognosis[1]. Further investigations on the etiology of PF are needed due to the increasing prevalence of this disease worldwide[2]. The annual incidence of PF is lower in South America and East Asia (less than 4 cases per 100,000 persons) compared to Europe and North America (3–9 cases per 100,000 persons)[3]. In 2011, the prevalence of PF in people aged 65 years and over was 494 cases per 100,000 persons and was more common in men[4–6]. Aberrant scarring is the defining feature of PF, leading to reduced lung capacity, diminished quality of life, and an average survival of 3–5 years from the time of diagnosis[2]. Inflammation leads to repetitive loss of repair and regulation following lung tissue damage, fibroblast proliferation, and extracellular matrix expansion, all of which are known to be the primary etiological factors of PF[7]. Lung transplantation is the sole fully curative

[1]Uyghur Medicines Hospital of Xinjiang Uyghur Autonomous Region, Urumqi 830049, P. R. China. [2]Department of Integrative Medicine, Huashan Hospital, Fudan University, Shanghai 200040, P. R. China. [3]Institute of Integrated Traditional Chinese and Western Medicine, Fudan University, Shanghai 200040, P. R. China. [4]Key Laboratory of Evidence-Based and Translation, Xinjiang Hospital preparation of Traditional Chinese Medicine, Urumqi, China. [5]Department of Integrated Traditional Chinese and Western Medicine, The Second Xiangya Hospital, Central South University, Changsha, China. [6]People's Hospital of Xinjiang Uygur Autonomous Region, Urumqi, China. [7]These authors contributed equally: Aman Gul and Yuanyuan Zhong. ✉email: lizhijian0220@sina.com; jcdong2004@126.com

option for PF, yet its feasibility was hindered by the lack of a reliable social support system[8]. Over the past 10 years, some pharmacotherapeutic agents, such as nintedanib and pirfenidone (a tyrosine kinase inhibitor), have demonstrated safety and efficacy in managing PF[9]. However, numerous side effects are associated with their use[10,11]. Thus, it is urgent to explore novel therapeutic agents that offer improved safety and efficacy for PF treatment.

Some active ingredients found in Traditional Chinese Medicine, including flavone derivatives, anthraquinones, alkaloids, polysaccharides, and terpenoids, have shown promising anti-pulmonary fibrotic efficacy, For instance, icaritin, a flavone derivative, has exhibited therapeutic potential against pulmonary fibrosis (PF) by inhibiting myofibroblast differentiation, potentially through PPARγ[12]. Barbaloin, a member of the anthraquinone family, possesses anti-fibrosis activity through the TGF-β1/Smads/p38 pathway[13]. Certain alkaloids, such as picrinine and scholaricine, have demonstrated protective properties against bleomycin (BLM)-induced PF by reducing collagen deposition via the MMP-1/TGF-β pathway[14]. Astragalus polysaccharides exhibit characteristics of multi-pathways and multi-targets, potentially regulating the expression of various genes, including *AHSA1*, *CASP3*, *CDK1*, *CDK2*, *HSP90AA1*, *JUN*, *NOS2*, *PTGER3*, *RELA*, *SOD1*, and *VCAM1* during the development of PF[15]. As a terpenoid, isoandrographolide has shown an anti-PF effect in silica-induced mice by reducing tubulointerstitial fibrosis, attenuating inflammatory responses, and protecting against kidney injury. Isoandrographolide has also exerted an inhibitory effect on tubular inflammation and epitheli-almesenchymal transformation. All of these effects are associated with the suppression of aberrant activation of the β-catenin/GSK-3β/AKT signaling, as supported by evidence from both experimental validation and network pharmacology analysis[16].

Rosmarinic acid (RA) is a polyphenolic compound widely found in plants of the Lamiaceae, Boraginaceae family. It is an active ingredient in different types of medicinal herbs, such as *Rosemary Rosmarinus officinalis*, *Sage Salvia officinalis*, and *Lemon Balm Melissa officinalis*[17–19]. RA possesses antioxidant, anti-inflammatory, anti-fibrotic, antitumor, and antimicrobial activities[20–29]. It exhibits superior antioxidative activity compared to vitamin E[30]. Previous clinical trials have demonstrated the efficacy of RA in treating asthma, allergies, and reactive airway disease[20,21,24–26]. In addition, the anti-fibrotic effect of RA has been observed in cardiac fibrosis[31], liver fibrosis[32], and renal interstitial fibrosis[33]. While several studies have explored the anti-fibrotic role of RA from various perspectives, both in rats and cells[29,34,35], few have investigated its correlation with a mouse PF model, and the underlying mechanism remains unclear.

Thus, in our study, a mouse model of BLM-induced PF was constructed using the intratracheal administration method, followed by 25 days of oral administration of RA. The curative effect of RA was validated using 4D label-free quantitative proteomics analysis. According to the results, RA at 40 mg/kg showed best efficacy to BLM-induced PF in mice. Proteomics and KEGG analysis indicated treatment of RA partially restored protein expression and activated the RAP1 signaling pathway, upregulating proteins like FGF1, Kit, Kras, and Src. With this study, we aimed to provide solid preclinical experimental evidence for the development of this novel and safe pharmacotherapeutic approach for the treatment of PF.

Materials and methods

Animals

Forty-eight male C57BL/6 mice (10–12 weeks old, $n = 8$ in each gloup) were obtained from Master of Shanghai Jesjie Laboratory Animal Co., Ltd. (SCXK2018-0004, Shanghai, China) and housed in a specific pathogen-free animal facility in accordance with the procedures approved by local ethics committee (2020-12-HSYY-DJC-01 and IACUC-20240226-06). All animals were given ad libitum access to food and water and maintained at 25 ± 2 °C under a 12-hour light/dark cycle. All experimental procedures were performed following local animal experiments regulations. After seven days of adaptive feeding, mice were randomly assigned into six groups: Control (CTL), Model (BLM), BLM + RA 20 mg/kg treatment (BLM + RA&L), BLM + RA 40 mg/kg treatment (BLM + RA&M), BLM + RA 80 mg/kg treatment (BLM + RA&H), and BLM + pirfenidone treatment (BLM + PFD). The study timeline was showed in Fig. 1. The study was reported in accordance with the ARRIVE 2.0 guidelines.

The mouse model of BLM-induced PF

BLM was obtained from Hanhui Pharmaceutical Co., Ltd. (Shanghai, China). After administering anesthesia with 50 mg/kg of pentobarbital sodium, the mouse model was established by intratracheal administration of 5 U/kg BLM using a quantitative intratracheal drug delivery device (Yuyan Instruments Co., Ltd. Shanghai, China). Before the PF modeling of mice, the mice were fasted for 12 h. Then, 2% pentobarbital (0.15 ml / 20 g) are injected intraperitoneally into the mice. The depth of anesthesia was checked by pinching the toes of the mice with forceps. When the mice were anesthetized, the hair on the neck of the mice was removed. After disinfection

Fig. 1. Diagram of the experimental protocol for rescue studies to test the effects of RA on BLM-induced pulmonary fibrosis mice. After BLM modeling for 3 days, mice received RA (20/40/80 mg/kg/d, i.g) or PFD (300 mg/kg, i.g) for 25 days until day 28. 0.9% saline was intragastrical administrated for control and model group mice.

with 75% alcohol, a longitudinal incision of approximately 0.5 centimeters is made on the skin of the neck with sterile surgical instruments, and then removed the subcutaneous tissue and exposed the trachea. After inserting the sterile 1-milliliter syringe needle at the upper edge of the first tracheal cartilage ring and withdrawing it, insert the quantitative nebulizer syringe into the needle hole on the airway for the injection of BLM (5 mg/kg) diluted with saline, or inject saline only. After the injection, the needle is immediately removed, the mouse is placed vertically and rotated for 3–4 min to ensure the uniform distribution of the drug in both lungs. After suturing, bandaging and cutting the neck incision, the mouse is placed on a side pad to make sure mouse regains consciousness and starts to act.

Treatment and euthanasia

From the third day after establishing the model, mice were administered with RA (20, 40, or 80 mg/kg, Chengdu Master Biotechnology Co., Ltd., China) or PFD (300 mg/kg, Med Chem Express LLC, NJ, USA) via oral gavage once daily for 25 days until day 28. The Model and Control groups received 0.9% normal saline daily by oral gavage.

At the end of the experiment, all mice were intraperitoneally injected with 2% pentobarbital (0.15 ml / 20 g) for anesthesia. Afterwards, the mice were euthanized by cervical dislocation.

Small-animal positron emission tomography-computed tomography (PET/CT) scanning

On Day 27, all mice underwent consecutive [18 F]-FDG-labelled small-animal PET/CT scans after intraperitoneal injection of 5MBq [18 F]-FDG PET/CT 60 min prior to imaging. Animals were kept under anesthesia (1.5% isoflurane) and positioned on a heated pad inside the Inveon MM PET scanner (Siemens, Japan). The images were processed and analyzed by the Inveon Research Workplace software (version 3.0; Siemens), and the mean standardized uptake value (SUV) for the lungs of each animal was calculated. The mean SUV was calculated as the ratio of MBq/mL (mean activity within each region of interest) to A0 (injected activity decay-corrected at the start of the PET acquisition [MBq] divided by the animal's weight [g]).

Pulmonary function test

Mice were anesthetized with 80 mg/kg of 2% pentobarbital via intraperitoneal injection and underwent tracheostomy using a standard catheter as previously described[36]. A forced pulmonary function testing system (Buxco, NY, USA) with the FinePointe and FinePoint Control Panel software was used for tracheostomy. Mice were positioned in the supine position on the bed inside the plethysmograph, mimicking the clinical pulmonary test commonly conducted on humans.

Classification and counting of leukocytes in bronchoalveolar lavage fluid (BALF)

BALF was harvested via endotracheal intubation with 300 μL of ice-cold phosphate-buffered saline (PBS) twice and centrifuged at 4 °C for 10 min at 500 g. The supernatants were then collected for enzyme-linked immunosorbent assay (ELISA). After resuspended with 50 μL of PBS, total cells were counted by an automated hematology analyzer (Model: BC-5000Vet, Mindray, Shenzhen, China).

ELISA

Mouse blood serum samples were centrifuged at 4000 rpm at 24 °C for 30 min, and the supernatants were collected. The levels of IL-6, TNF-α, TGF-β1, and IL-1β in the serum and BALF samples were determined using ELISA kits (WellBio Technology Co., Ltd., Shanghai, China).

Histological analysis

After euthanasia, mouse lung tissues were immediately fixed in 4% paraformaldehyde and embedded in paraffin. Then, the blocks were sectioned at 5 μm using a microtome. Masson's trichrome staining and hematoxylin & eosin (H&E) staining were performed to analyze the inflammation and collagen fiber deposition in the trachea and lung collagen fiber areas.

4D label-free quantitative proteomics analysis

Mouse lung tissues were lysed, and the protein was extracted using SDT buffer (pH = 7.6, 100 mM Tris-HCl, 4% SDS). The protein concentration was quantified using BCA protein assay kit (Bio-Rad, USA). Each protein sample (20 μg) was mixed with 5× loading buffer and boiled for 5 min. Protein samples were separated on a 4–20% SDS-PAGE gel (45 min, constant voltage 180 V) and visualized by Coomassie Blue R-250 staining. Proteins were digested by trypsin following the filter-assisted sample preparation procedure reported by Matthias Mann. The resulting digestion peptides were desalted on C18 cartridges (Empore™ SPE Cartridges C18, volume 3 mL, standard density, bed I.D. 7 mm, Sigma-Aldrich), concentrated by vacuum centrifugation, and reconstituted in 40 μL of 0.1% (v/v) formic acid. A tims TOF Pro mass spectrometer (Bruker) coupled to Nanoelute (Bruker) was used for LC-MS/MS analysis. Peptides were applied to a C18 reversed-phase analytical column (Thermo Scientific Easy Column, inner diameter: 75 μm, length: 25 cm, 1.9 μm resin) in 95% buffer A (0.1% formic acid in water) and separated with a linear gradient of buffer B (0.1% formic acid and 99.9% acetonitrile) at a flow rate of 300 nL/min. The positive ion mode with an applied electrospray voltage of 1.5 kV was selected for mass spectrometer. Fragments and precursors were analyzed at the TOF detector over a mass range of m/z 100–1700. The tims TOF Pro was operated in the parallel accumulation-serial fragmentation mode with ion mobility coefficient (1/K0) set from 0.6 to 1.6 Vs cm2 (1 MS and 10 MS/MS parallel accumulation-serial fragmentation scans). The active exclusion was enabled with a release time of 24 s. Raw MS data for each sample were combined and searched using the MaxQuant 1.6.14 software for quantification and identification analysis. Gene ontology (GO) terms were mapped, and sequences were annotated using the Blast2GO software. R scripts

were used to plot GO annotation results. The Kyoto Encyclopedia of Genes and Genomes (KEGG) database (http://geneontology.org) was used to retrieve KEGG ortholog identifications, which were then mapped to pathways in KEGG. The proteomics experiment was performed by Shanghai Applied Protein Technology Co., Ltd.

Western blotting

Frozen lung tissues were minced and lysed in RIPA buffer supplemented with a protease inhibitor cocktail, including phosphatase inhibitors, protease inhibitors, and phenylmethanesulfonyl fluoride. The concentration of total protein was quantified using BCA protein assay kit (Shanghai Wei'ao Biotech Ltd. WB0123 and WB2123). Subsequently, protein samples were separated by 10% SDS-PAGE (30 μg protein in each well) and transferred onto 0.2-μm PVDF membranes. The blots were blocked with 5% bovine serum albumin for 2 h at ambient temperature and then stained with anti-Src (1:1000, 320001, ZEN-BIOSCIENCE), anti-FGF1 (1:1200, R24301, ZEN-BIOSCIENCE), anti-Kras (1:1000, DF6324, Affinity), anti-C-kit (1:1000, 347321, ZEN-BIOSCIENCE), and anti-GAPDH (1:2000, WB2197, WEIAO) antibodies at 4 ℃ overnight. Subsequently, the blots were incubated with HRP-conjugated goat anti-rabbit antibodies (1:2000, WB2177, WEIAO) for 2 h at ambient temperature. The protein bands were visualized by an ECL chemiluminescence detection system and quantified by the Image J software.

Immunohistochemistry (IHC) staining

After dewaxing, hydration, and antigen retrieval, lung tissue sections were blocked with 3% bovine serum albumin and then stained with anti-Src (1:100), anti-FGF1 (1:50), anti-Kras (1:100), and anti-C-Kit (1:100) antibodies at 4 ℃ overnight. After three washes with PBS, the slides were incubated with a goat anti-rabbit IgG secondary antibody at 37 °C for 50 min. Subsequently, DAB (G1211, Servicebio, 166, China), chromogenic reaction, and hematoxylin counterstaining were performed. Lastly, the slides were mounted with coverslips and examined under a light microscope (100×). The Image Pro Plus 6.0 software was used to measure and analyze five views on each slide.

Molecular docking simulation

To validate compound-target associations, we used the AutoDock software (version 4.2) to run molecular docking program[37]. The 3D structure files of key target proteins were retrieved from RCSB PDB (https://www.rcsb.org). The 3D structure files of compounds were obtained from PubChem (https://pubchem.ncbi.nlm.nih.gov). The AutoDock platform was then used for molecular docking verification. Binding energy less than "−5" indicated a good binding interaction between the compound and the target[38]. The binding site and ligand docking were visualized and analyzed using PyMOL and Auto-Dock Vina[39].

Statistical analysis

The GraphPad Prism (8.0) software was used for statistical analysis of the experimental data. All results were presented as mean ± standard deviation (SD). The homogeneity of variance test and normality test were performed on measurement data. One-way ANOVA was used to compare data that were consistent with homogeneity of variance and normal distribution. Tukey test was used for pairwise comparisons among multiple groups. A significance level of $p < 0.05$ was considered statistically significant. #$p < 0.05$, ##$p < 0.05$, ###$p < 0.005$, ####$p < 0.001$ vs. Control group; *$p < 0.05$, **$p < 0.01$, ***$p < 0.005$, ****$p < 0.001$ vs. BLM group.

Results

RA alleviates BLM-induced PF in mice

Compared to the Control group, the lung CT scans of BLM-treated mice exhibited extensive patchy fibrous cords and even areas of consolidation on Day 17. The patchy and fibrous cord shadows were markedly decreased, and the degree of fibrosis was decreased in the axial and coronal planes of both the BLM + RA and PFD groups (Fig. 2A and C). Compared with the Control group, the reduced aeration caused by BLM was significantly reversed by both RA and PFD, especially by RA at a dose of 40 mg/kg, but not in the BLM + RA (10 mg/kg) group (Fig. 2E). The results of PET/CT scans demonstrated that the[18] F-FDG uptake in the lung tissues of the BLM group was significantly higher than that in control animals, while RA treatment notably decreased the[18] F-FDG uptake in the lungs. The average SUV of the BLM group was significantly increased in comparison with the Control group, while RA treatment decreased this value in model mice (Fig. 2B and D, and 2F).

RA alleviates lung function damage induced by BLM

Body weight was recorded every seven days until the mice were euthanized. As results shown in Fig. 3A, mice exhibited a significant loss of body weight after the instillation of BLM. However, RA or PFD treatment reversed the weight loss of mice after 25 days of treatment. The pulmonary function test on Day 28 showed that the FVC, Cchord, PEF, VC, IC, and MMEF of the BLM group were significantly decreased in comparison with the controls. Treatment with RA and PFD resulted in a notable increase in the above six indicators (Fig. 3B-G).

RA attenuated BLM-induced pulmonary inflammation

Inflammatory cell counting and ELISA were performed to evaluate the anti-inflammatory effect of RA. Significant infiltration of inflammatory cells was observed in the lungs of BLM-treated mice, including neutrophils, lymphocytes, monocytes, eosinophils, and basophils ($p < 0.001$, Fig. 4A-F). Both RA and PFD treatments significantly reduced cell populations, especially at the 30 mg/kg dosage of RA. In addition, the levels of inflammatory cytokines (i.e., TGF-β1, IL-1β, TNF-α, and IL-6) in BALF were significantly increased in the BLM group as compared to the controls. After treatment with RA or PFD, the levels of inflammatory cytokines

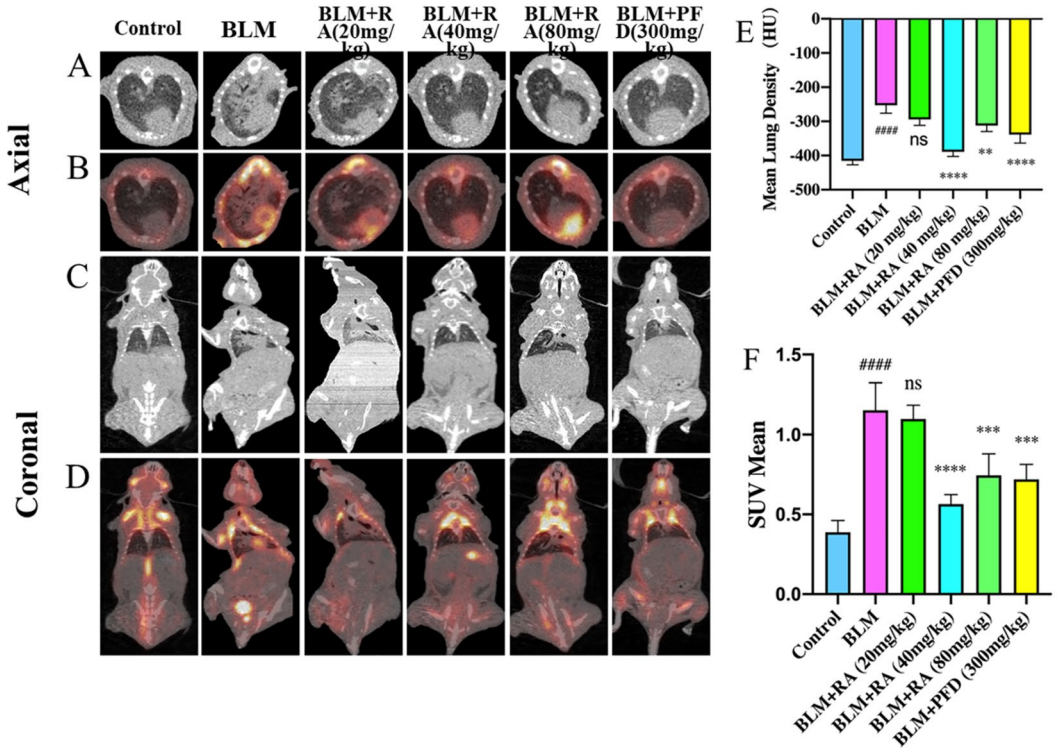

Fig. 2. RA alleviates BLM-induced pulmonary fibrosis in mice evaluated via PET/CT. **A** Representative CT images of the horizontal plane. **B** Representative PET/CT images of the horizontal plane. **C** Representative CT images of the coronal plane. **D** Representative PET/CT images of the coronal plane. **E** Mean lung density of Control, BLM, BLM + RA(20/40/80 mg/kg), BLM + PFD groups. **F** Lung SUV mean of Control, BLM, BLM + RA (20/40/80 mg/kg), BLM + PFD groups. Data were represented as mean ± SD. $n = 4$ mice/group, #### $p < 0.001$ vs. Control group, $^{*}p < 0.05$, $^{**}p < 0.01$, $^{***}p < 0.005$, $^{****}p < 0.001$ vs. BLM group.

were markedly decreased in model animals (Fig. 4G-J). Similar results were in observed in serum inflammatory cytokines (i.e., TGF-β1, IL-1β, TNF-α, and IL-6) after RA or PFD treatment (Fig. 4K-N). These findings suggest that RA may attenuate BLM-induced lung inflammation.

RA alleviates BLM-induced pulmonary fibrosis in mice

To assess the anti-fibrotic and anti-inflammatory effects of RA on BLM-induced PF, we analyzed mouse's lung tissue sections using Masson's trichrome staining and H&E staining (Fig. 5). Similar to PFD treatment, RA effectively reversed BLM-induced collagen deposition and inflammatory cell infiltration, not only in the interstitial and airway circumambient areas but also in the vessels, as compared to the controls (Fig. 5A). Treatment with PFD or RA at a dosage of 40 or 80 mg/kg resulted in a remarkable reduction in the overall inflammation score and collagen fiber area compared with those treated with saline. However, mice treated with RA at 20 mg/kg did not show the same level of improvement (Fig. 5B-C), as low dosage might not have been sufficient to achieve the desired therapeutic effect.

Differentially expressed proteins (DEPs) identified by 4D label-free quantitative proteomic analysis

To investigate the therapeutic mechanism of RA on BLM-induced PF, we extracted the proteins from lung tissues of the Control, BLM, and BLM + RA&M groups. After the proteomics quality control analysis of the extracted proteins (Figure S1 & Figure S2), we conducted 4D label-free quantitative proteomics analysis of the Control, BLM, and BLM + RA&M groups. Principal component analysis showed a distinct separation of the BLM group from the Control group, while RA&M treatment partially reversed this separation (Fig. 6A). To identify DEPs between the three groups, we used fold change and p-value (T-test) as the criteria to create a volcano map. Significantly downregulated proteins were marked in blue ($p < 0.05$ and FC < 0.5), while significantly upregulated proteins were shown in red ($p < 0.05$ and FC > 2.0). Unaltered proteins were presented in grey (Fig. 6B-C). Proteomics analysis demonstrated that BLM induction significantly upregulated 418 proteins and downregulated 352 proteins in comparison with the Control group (Fig. 6D). RA&M treatment, however, reversed the expression of 459 proteins compared to the BLM (Model) group, with 252 upregulated proteins

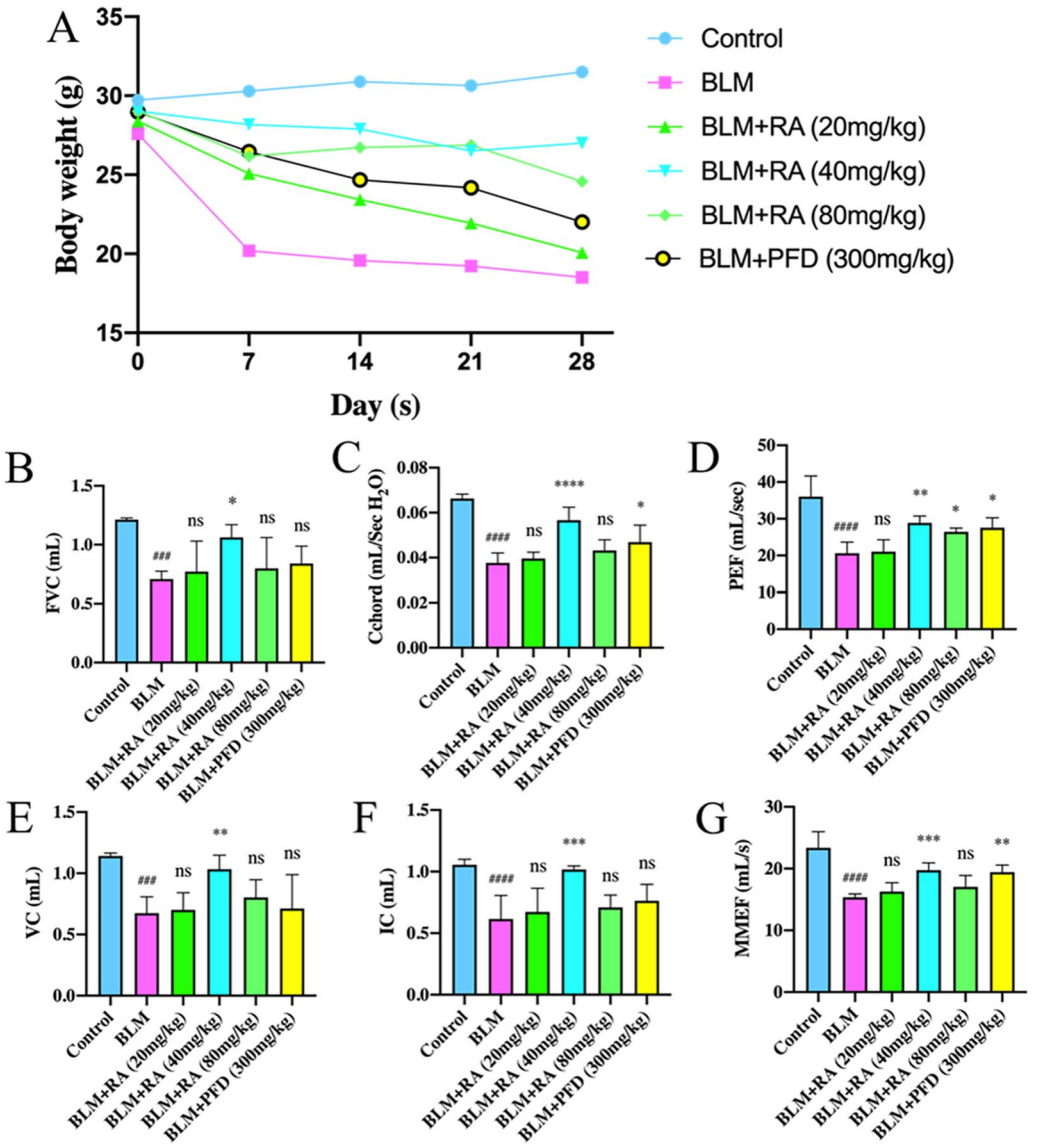

Fig. 3. RA alleviates lung function damage induced by BLM. **A** Body weight changes were recorded. **B**–**G** Pulmonary function tests (FVC, Cchord, PEF, VC, IC, and MMEF) were measured. Data were represented as mean ± SD. $n = 4$ mice/group, #### $p < 0.001$ vs. Control group, $^{*}p < 0.05$, $^{**}p < 0.01$, $^{***}p < 0.005$, $^{****}p < 0.001$ vs. BLM group.

and 217 downregulated proteins (Fig. 6E). The heat map displays 459 overlapping DEPs directly regulated by RA (Fig. 6F).

Bioinformatics analysis of DEPs regulated by RA in BLM-induced PF model

Based on the 469 DEPs (Supplementary materials, Table S1), GO and KEGG pathway enrichment analyses were performed. The top 20 GO terms suggested that the molecular function cellular component, and biological process of DEPs were mainly related to cell function, cell biological adhesion, and cell membrane (Fig. 7A). Pathway enrichment analysis identified 20 enriched pathways, including the N-glycan biosynthesis, tight junction, and RAP1 signaling pathways between the BLM + RA&M and BLM groups (Fig. 7B). Subsequently, we examined the proteins involved in the KEGG pathway at level 2, and the results showed that RAP1 may be the primary signaling pathway regulated by RA (Fig. 7C). The protein-protein interaction network (Fig. 7D) and heatmap (Fig. 7E) display the 22 most enriched proteins in the RAP1 signaling pathway among the Control, BLM, and BLM + RA&M groups. We further focused on four DEPs related to cell adhesion and proliferation, including FGF1, Kit, Kras, and Src (Fig. 7F). The data of Rap1 signaling pathway (map04015) was from KEGG (Kyoto Encyclopedia of Genes and Genomes)[40]. They have exhibited potential regulatory effects on actin cytoskeleton, focal adhesion, proliferation survival gene activation, cell adhesion, migration, and polarity. Based on these findings, we hypothesized that FGF1, c-Kit, Kras, and Src could serve as therapeutic targets of RA in the treatment of PF (Table 1).And the molecular docking analysis revealed that RA&M exhibited favorable

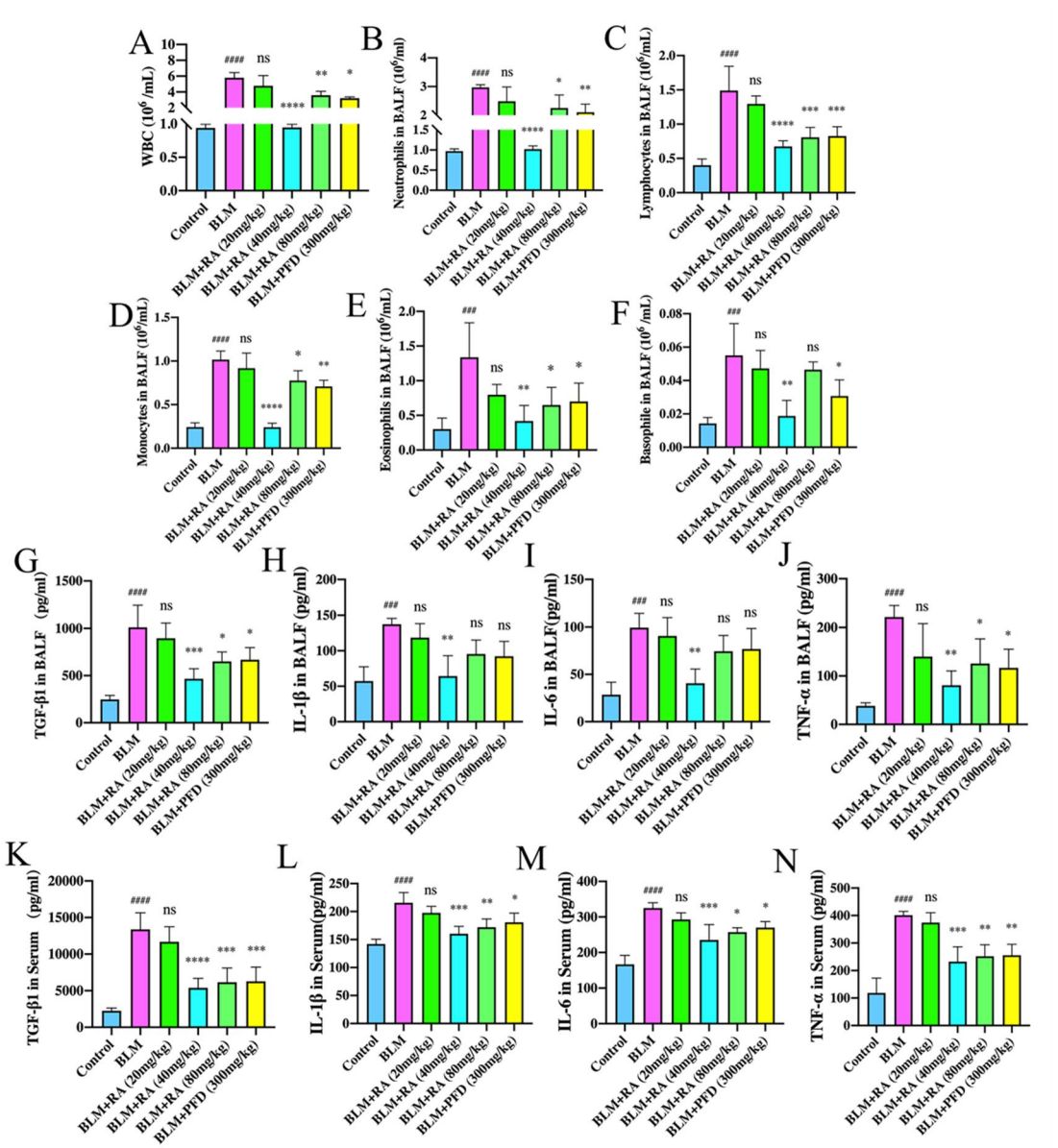

Fig. 4. RA restored lung inflammatory response induced by BLM. **A**–**F** Inflammatory cells count (neutrophils, lymphocytes, monocytes, eosinophils, and basophils) in bronchoalveolar lavage fluid (BALF). **G**–**J** Pro-inflammatory cytokines (IL-1β、IL-6、TNF-α, TGF-β1) in bronchoalveolar lavage fluid (BALF). **K**–**N** Pro-inflammatory cytokines (IL-1β、IL-6、TNF-α, TGF-β1) in serum. Data were represented as mean ± SD. $n = 4$ mice/group, #### $p < 0.001$ vs. Control group, $^{*}p < 0.05$, $^{**}p < 0.01$, $^{***}p < 0.005$, $^{****}p < 0.001$ vs. BLM group.

compound-target interactions with FGF1, c-Kit, Kras, and Src, with binding energy less than − 5.0 kcal/mol (Fig. 8). Besides, the results of molecular dynamics simulation showed that the structures of the complexes formed by the 4 proteins (c-Kit, Src, FGF1, Kras) with RA change stably over 0-100 nanoseconds (Figure S3 & Figure S4).

RA reversed the downregulation of FGF1, c-Kit, Kras, and Src in mouse lung tissues possibly by activating the RAP1 signaling pathway

To provide further insights into the results of proteomics analysis, we performed Western blotting and IHC staining to examine the protein expression levels of key DEPs (FGF1, c-Kit, Kras, and Src, Fig. 9A-E). Consistently, the protein levels of FGF1, c-Kit, Kras, and Src were significantly decreased in the BLM group compared with the controls (all $p < 0.05$), while RA&M treatment reversed these changes (all $p < 0.05$) (Fig. 9A-E). IHC staining also confirmed the expression trends of these proteins (Fig. 9F-J). Collectively, these findings indicate that activation of the RAP1 signaling pathway by RA plays an important role in alleviating BLM-induced PF.

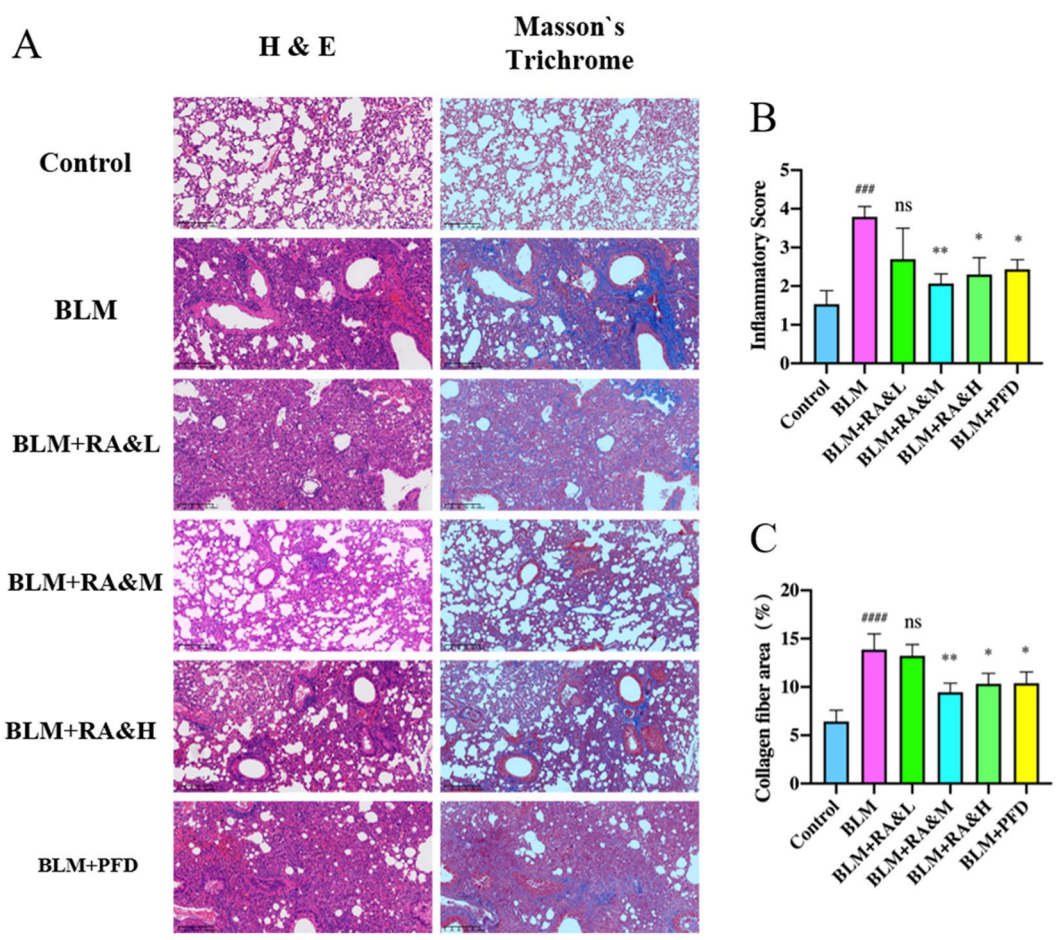

Fig. 5. RA alleviated BLM-induced pulmonary fibrosis in mice evaluated via H&E and Masson`s trichrome staining. **A** The representative images of H&E and Masson staining in six groups with 100x. **B** Quantitative inflammatory score of H&E staining. **C** Quantitative results of collagen fiber area in Masson staining. Data were represent as mean ± SD. $n = 4$ mice/group, #### $p < 0.001$ vs. Control group, $^{*}p < 0.05$, $^{**}p < 0.01$, $^{***}p < 0.005$, $^{****}p < 0.001$ vs. BLM group.

Discussion

PF is a life-threatening disease with patients typically surviving only 3–5 years after diagnosis. The exact cause of PF remains unclear, and current pharmacotherapy options have proven to be ineffective. A series of pathological changes related to PF, such as early and recurrent inflammation, oxidative stress, fibroblast proliferation, extracellular matrix expansion, myofibroblast proliferation, and fibrosis, all of which require more effective and novel treatment approaches[41]. In the present work, we used a mouse model of BLM-induced PF to evaluate the therapeutic potential of RA and explored the underlying mechanisms using 4D label-free quantitative proteomics. Our research firstly demonstrated how RA functions as an anti-inflammatory and anti-fibrotic agent in the treatment of PF.

BLM was initially discovered in 1962 and first reported in 1966[42]. It is a chemotherapeutic agent widely used to treat various neoplastic diseases, such as lymphoma, ovarian cancer, testicular cancer, head and neck squamous cell carcinoma, and malignant pleural effusion. One of the most serious side effects of BLM in clinical use is lung toxicity. Previous studies have extensively investigated the development and progression of PF by revealing the mechanisms of BLT. At present, BLM administration has become the most widely used method to establish PF in experimental animals[43]. Here, we constructed a mouse model of BLM-induced PF. Three days later, mice were treated with RA at three dosages or PFD for 25 days. The results demonstrated that RA significantly improved lung function, reduced body weight loss, and exhibited an anti-inflammatory effect, as evidenced by reduced cell counts in both serum and BALF samples and decreased inflammation scores in H&E staining (Figs. 2, 3, 4 and 5). Proinflammatory cytokines, such as IL-1β, TNF-α, and IL-6 play a pivotal role in fibrogenesis by regulating immune cell recruitment, fibroblast activation, and the expression of TGF-β1, a key profibrotic cytokine[44]. In our study, RA not only alleviated immune cell accumulation in lung tissues but also decreased the levels of these cytokines, suggesting its potential as a novel drug for PF treatment. To further elucidate the underlying mechanisms and potential targets of RA, we performed 4D label-free quantitative proteomics analysis. A total of 770 proteins were quantified when comparing healthy and pulmonary fibrotic mice, while 669 DEPs were

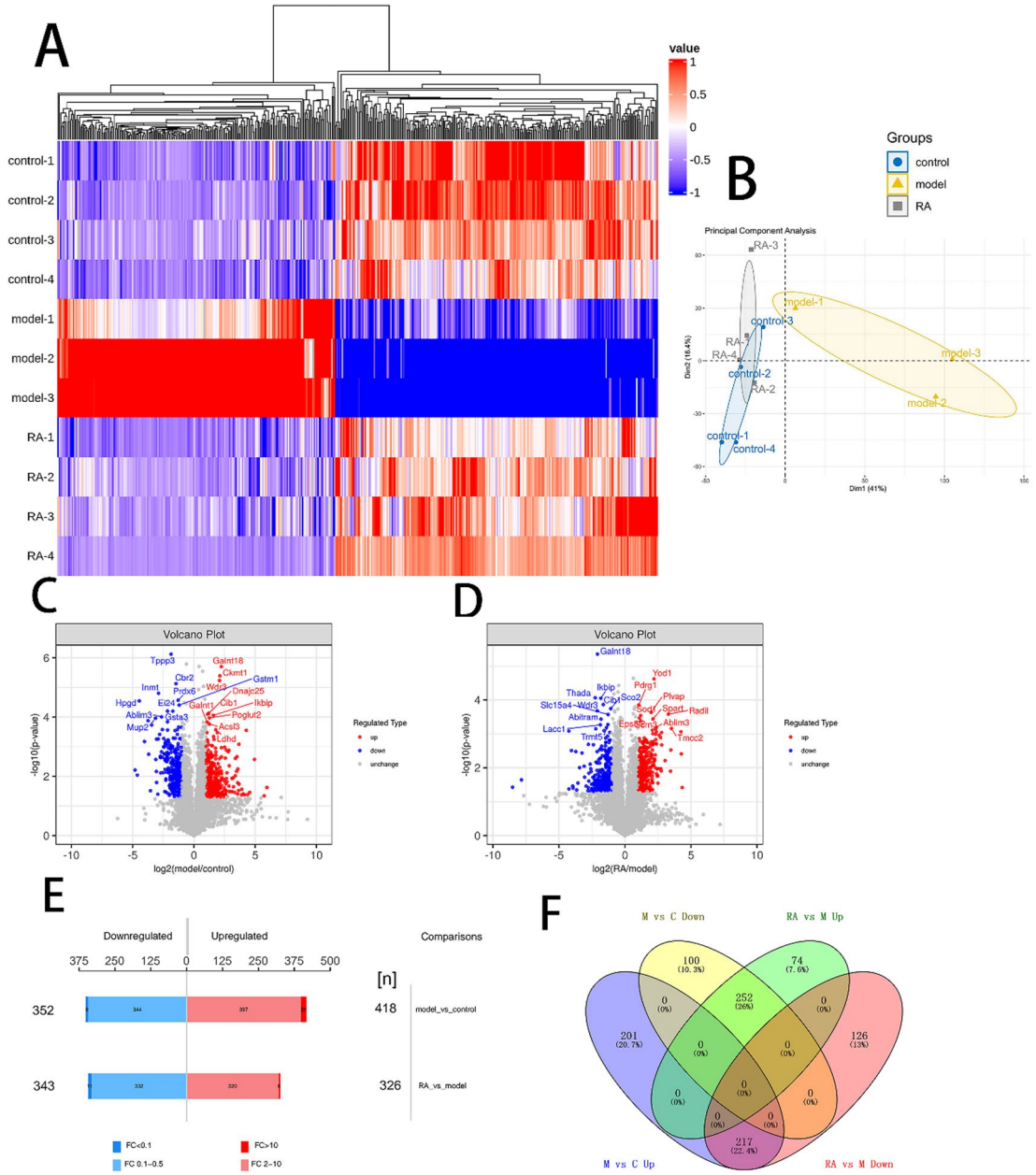

Fig. 6. DEPs in lungs between Control, BLM, and BLM + RA&M groups identified by 4D Label-free Quantitative Proteomic analysis. **A** Principal component analysis (PCA) of Control, BLM, and BLM + RA&M groups based on identified proteins. **B**, **C** Volcano plot of identified proteins (especially significantly changed proteins) in BLM vs. Control and BLM + RA&M vs. BLM, Red, and Blue indicated significantly upregulated or downregulated proteins. **D** Histogram of protein quantitative difference results between Control, BLM, and BLM + RA&M groups. **E** Venn diagrams showing the distribution of overlapping proteins among Control, BLM, and BLM + RA&M groups. **F** Heatmap of the DEPs.

identified in RA&M-treated mice. Notably, 469 DEPs overlapped when comparing the three groups (Fig. 6). Based on the results of level 2 KEGG pathway enrichment and protein-protein interaction network analysis, we speculated that RA might regulate several signaling pathways, including protein processing in the tight junction, endoplasmic reticulum, and the RAP1 signaling pathway during the progression of PF (Fig. 7). Meanwhile, RA may regulate the signaling pathways of DEPs, such as FGF1, Kit, Kras, and Src, which are closely related to the pathogenesis of PF.

Our proteomics analysis identified FGF1, c-Kit, Kras, and Src as key regulators involved in cell survival and proliferation, cell differentiation and migration, cell adhesion and immune responses, and connective tissue deposition. FGF1, also known as acidic Fgf1[45], is a mammalian fibroblast growth factor with significant importance in the maintenance and proliferation of ACEs. Maitre et al. showed that overexpression of FGF1 by adenoviral vector transfection induced the proliferation of AECs and exerted a beneficial effect on hyperoxic

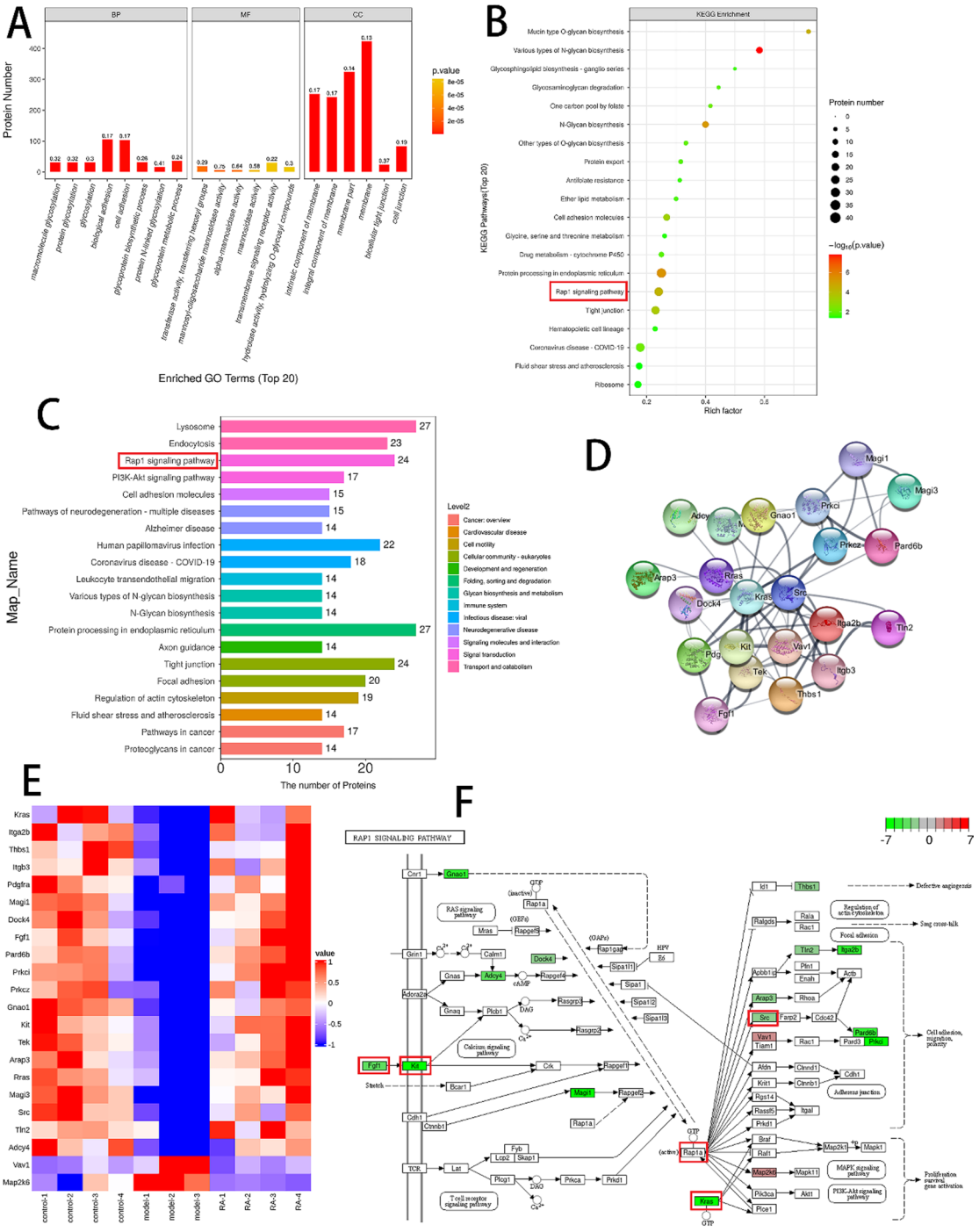

Fig. 7. Bioinformatics analysis of 469 DEPs regulated by RA in BLM-induced PF model. **A** GO term performance analysis of DEPs between BLM + RA and BLM groups. **B** The top 20 enriched KEGG pathways. **C** KEGG pathway annotation and attribution bar chart. The horizontal axis represents the number of pathway protein annotations, and the vertical axis represents the KEGG annotation names. The colors represent the KEGG channels at level 2. **D** Protein-protein interaction network (PPI) of 22 proteins enriched in the RAP1 signaling pathway. **E** Heatmap of 22 proteins enriched in RAP1 signaling pathway between Control, BLM, and BLM + RA&M groups. **F** KEGG pathway map of RAP1 signaling pathway and involved proteins between BLM + RA&M and BLM groups (Rad mark indicated reversed main DEPs by RA).

lung injury in rats[46]. FGF1 has also been shown to induce apoptosis and reduce the production of smooth muscle actin[47]. FGF1 also protected AECs from injury when exposed to TGF-β1, contributing to preserving the basement membrane during the pathogenesis of PF[48–51]. Shimbori et al. reported that FGF1 not only inhibited lung fibrosis but also decelerated the progression of existing fibrosis in mice. Activating the FGF1 pathway may

Protein ID	Gene	Peptides	Control vs.BLM (model)			BLM + RA vs. BLM (model)		
			P value	Ratio	Type	*P* value	Ratio	Type
P61148	FgflP	3	0.002	0.346	Down	0.007	3.368	Up
P05532	c-Kit	8	0.011	0.259	Down	0.009	4.066	Up
P32883	Kras	5	0.038	0.293	Down	0.041	3.351	Up
P05480	SRC	15	0.005	0.387	Down	0.015	2.111	Up

Table 1. Key DEPs regulated by RA.

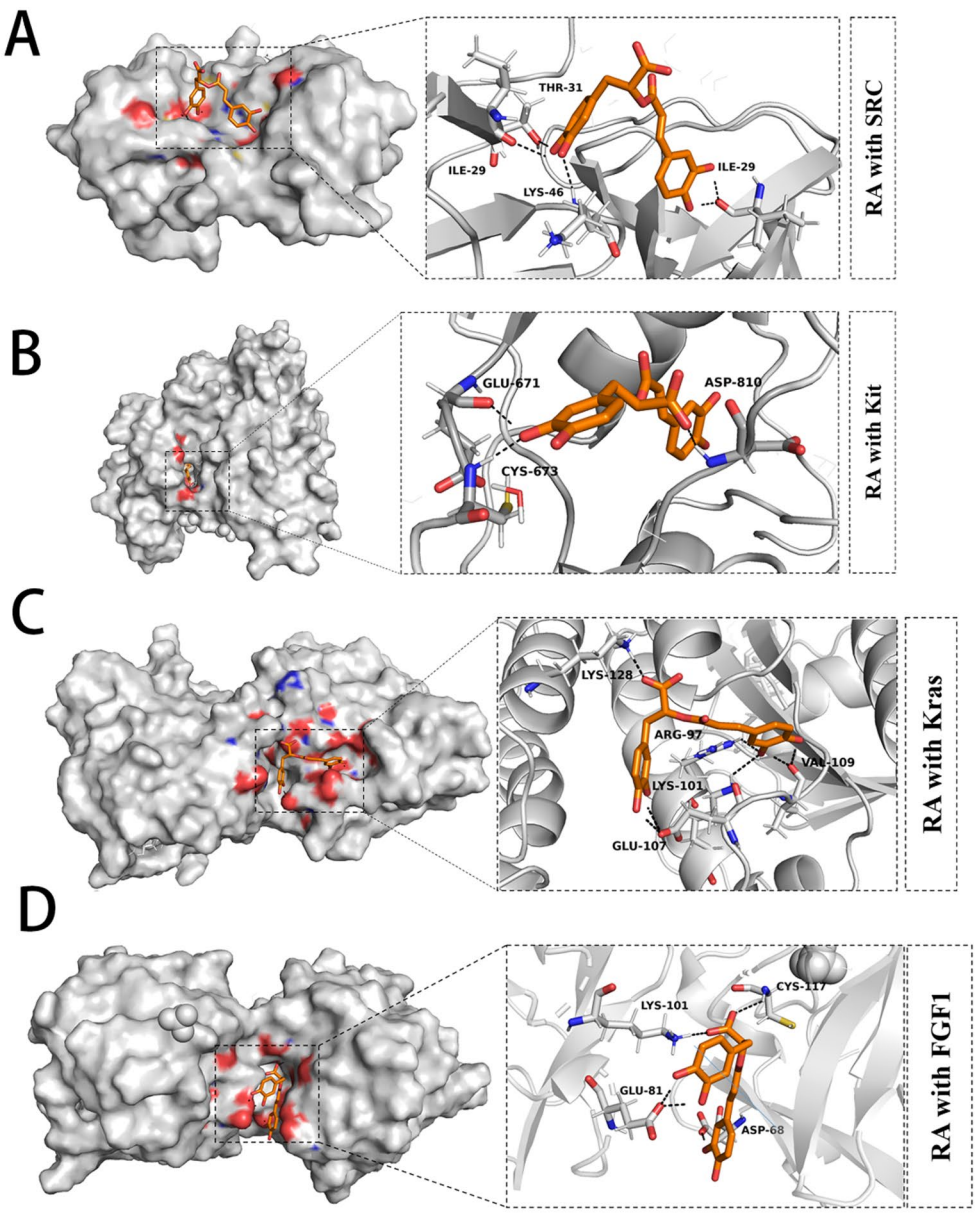

Fig. 8. The predicted binding sites of RA with Src, Kit, Kras and FGF1. **A** The predicted binding sites of RA with SRC (PDB ID: 5NVJ, binding energy: – 7.078). **B** The predicted binding sites of RA with Kit (PDB ID: 4U0I, binding energy: -10.81(ΔG, kcal/mol)). **C** The predicted binding sites of RA with Kras (PDB ID: 6GJ5, binding energy: – 5.767). **D** The predicted binding sites of RA with FGF1 (PDB ID: 1JT5, binding energy: – 5.99).

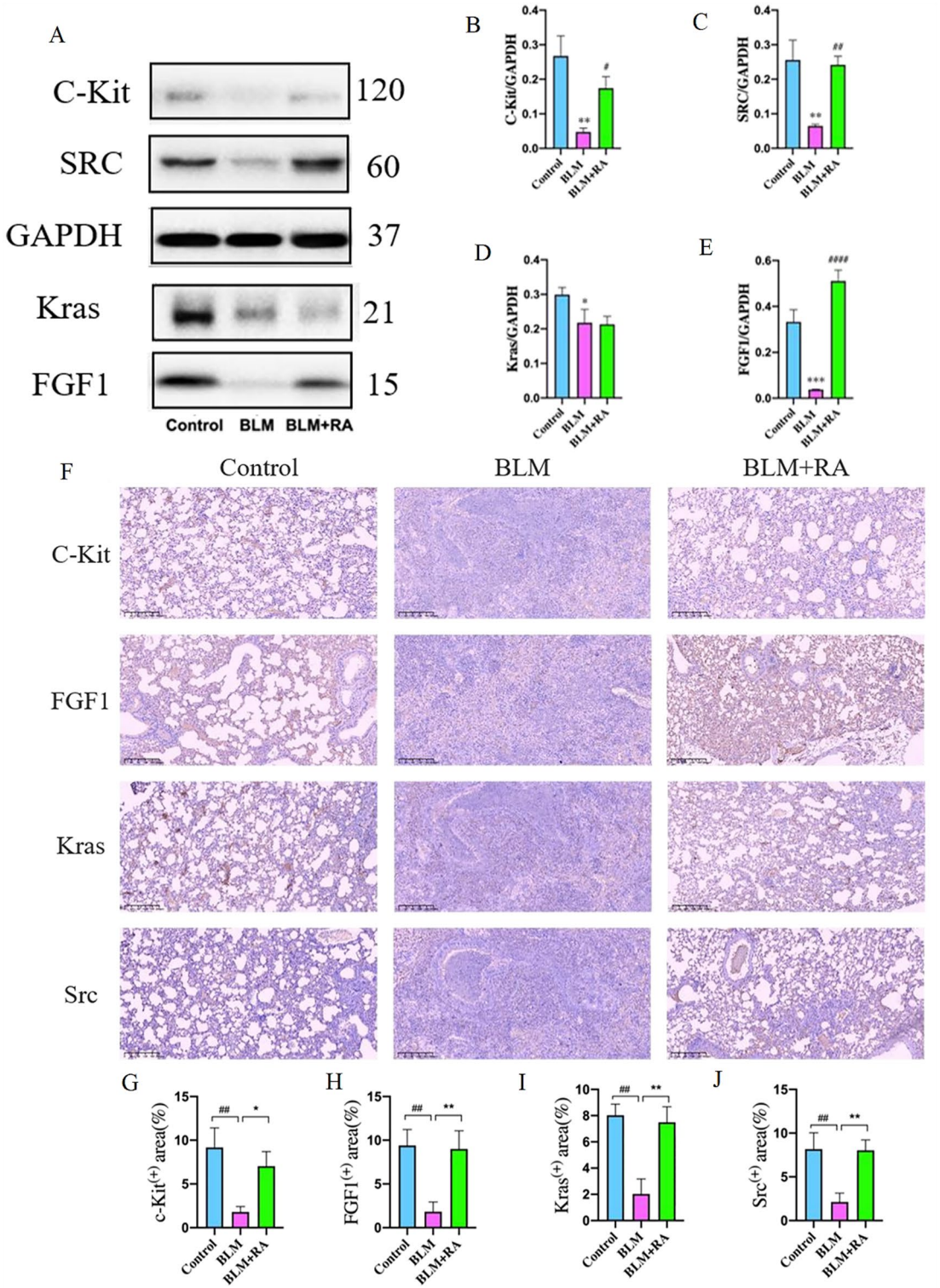

Fig. 9. RA inhibited BLM-induced pulmonary fibrosis by activating the RAP1 signaling pathway **A** Western blot images of C-Kit, Src, FGF1, Kras. **B**–**E** quantitative analysis. **F** representative images of IHC examination for C-kit, FGF1, Kras, and Src. **G**–**J** Positive expression of C-Kit, FGF1, Kras, and **E** Src. Data were represented as mean ± SD. $n = 4$ mice/group, #$p < 0.05$, ##$p < 0.01$, ###$p < 0.005$, #### $p < 0.001$ vs. Control group, *$p < 0.05$, **$p < 0.01$, ***$p < 0.005$, ****$p < 0.001$ vs. BLM group.

be a beneficial strategy for the development of improved and well-balanced anti-fibrotic therapies[52]. What's more, *FGF1* was a Rap1 pathway related gene, which can regulate the Rap1 pathway by high expression[53].

Stem cell factor receptor Kit protein, also known as c-Kit proto-oncogene or CD117, encodes a receptor tyrosine kinase (RTK)[54]. It is a well-known target for several anti-neoplasm agents, such as Imatinib[55], Sunitinib[56], Regorafenib[57], Ripretinib[58], and Avapritinib[59]. However, a phase 2 clinical trial of imatinib for the treatment of PF patients failed, and the underlying reason for this remains unclear[60]. Kit is a receptor protein expressed by many types of cells, including resident cells with stem/progenitor characteristics and distinct regional features, basal cells and their derivatives cells[61,62], lung-derived mesenchymal cells[63], Clara cells and their variants[64], alveolar epithelial type II progenitor cells[65], and c-Kit(+) stem cells[66,67], especially during the maintenance of the homeostasis and the repair phase of cell injury[68]. In our study, mice with BLM-induced PF were euthanized at Day 28, which is known as the fibrotic and repair phase[69]. The c-Kit is essentially a transmembrane protein and located at the upstream of Rap1 pathway[70]. Besides, FGF1 was reported to target the receptor tyrosine kinases, which including the c-kit[71].

Kras is a member of the small GTPase superfamily, belonging to the mammalian Ras gene family[72]. Kras, Nras, and Hras are the three major RAS isoforms that tend to mutate in human cancers[73]. There are two isoforms of Kras: Kras-4 A and Kras-4B. Kras-4B is the dominant isoform in human cancers. It is found in nearly 90% of pancreatic cancers, 30–40% of colorectal cancers, and 15–20% of lung cancers[74]. Castellano and Downward et al. have reported that membrane recruitment involves direct binding to GEFs and GAPs, leading to their activation and translocation, which is a critical step in Kras mutation and pathogenicity[75–77]. Kras regulates a multitude of cellular processes, including cell differentiation, apoptosis, and proliferation[78]. Ogawa et al. have reported that upregulation of Kras plays a positive role in lung injury[79]. Besides, MEK is a canonical effector of Kras[80]. While the Rap1/MEK/ERK signaling pathway was a major target to alleviate fibrosis effectively[81]. Consistently, we found that Kras was downregulated in BLM-treated mice, but was upregulated after RA treatment, suggesting the therapeutic effect of RA at both gene and protein levels.

The non-receptor tyrosine kinase Src belongs to the Src family kinases. Among all family members, Src is the only one that is ubiquitously expressed[82]. Gao et al. have reported Src was located at the downstream of RAP1[83]. However, Src activation is also implicated in the pathogenesis of many diseases, such as cancers[84], HIV/AIDS[85], neurodegenerative diseases[86], epilepsy[87], and fibrosis diseases[88]. The fibrogenic effect of Src kinases has been confirmed by the anti-fibrotic activity of SU6656, a specific Src kinase inhibitor[89]. However, the mechanisms underlying the maintenance of a normal or fibrotic lung microenvironment and the factors determining the outcome of PF remain unclear. Our study provided some evidence regarding the therapeutic role of RA in mice with BLM-induced PF.

According to the previous research, there are numerous therapeutic drugs for liver fibrosis in clinical practice, and their mechanisms of action vary greatly. Inhibiting the TGF-β pathway is a major approach in drug development. For example, PFD alleviates pulmonary fibrosis in vitro and in vivo through regulating TGF-β1 pathway[90]. Recently, the thyroid hormone receptor-β (THR-β) analogue Resmetirom, a metabolic regulator, has shown remarkable performance in clinical trials, significantly improving liver fibrosis and becoming the first drug approved by the FDA for the treatment of non-alcoholic steatohepatitis (NASH) accompanied by moderate to severe liver fibrosis[91]. In our research, RA alleviates pulmonary fibrosis by regulating the Rap1 pathway with different ways: FGF1-c-Kit-RAP1-Src- cell adhesion migration, or FGF1-c-Kit-RAP1-ERK-MAPK- cell proliferation survival, or Kras–ERK-MAPK- cell proliferation survival. Compared with PFD, Resmetirom, the mechanism of RA in treating liver fibrosis has the characteristic of multiple targets. Due to the complex mechanism of liver fibrosis, RA has greater potential for application.

However, although our work has got some results in the research on the mechanism of RA in anti-fibrosis, there are still some limitations in our study. Firstly, the complexes formed by RA and FGF1, c-Kit, Kras, and Src were derived from bioinformatics analysis, we need SPR or CETSA to verify the bindings. The data of SPR or CETSA can better support our conclusion. Secondly, we concluded that the RAP1 pathway is a key target for RA, based on our results. However, we did not verify the direct effects of overexpression or silencing of the rap1 gene on the action of RA. It is meaningful to conduct functional validation of the RAP1 gene at the cellular level. And we are planning to carry the functional verification in the future research. Thirdly, further confirmation of RA's physiological toxicity is necessary. For instance, evaluations of liver and kidney functions in mice treated with RA are crucial for the clinical development of RA. But we didn't concern about this. What's more, we also lack the long-term results of the RA treatment in mouse PF model. With the consideration of these, we are planning to investigate the chronic toxicity assessment in the future work.

Our study confirmed that RA regulated the protein expressions of FGF1, c-Kit, Kras, and SRC, as evidenced by the results of Western blotting, and IHC staining. This regulatory process appears to involve the RAP1 signaling pathway (Figs. 7, 8, 9 and 10). We proposed that the initial cell injury caused by BLM impeded cell repair process, resulting in the downregulation of proteins related to cell repair. In addition, RA treatment suppressed the release of cytokines mediated by NK cells, T cells, neutrophils, and B cells (Fig. 4), which may be related to the activation of the RAP1 signaling pathway by RA. The potential binding sites between RA and FGF1, Kit, Kras, and Src were then simulated to further validate their significant roles in the therapeutic effects of RA in BLM-induced PF (Figs. 7, 8 and 10). As our research continues, we aim to determine whether these proteins directly mediate the therapeutic effect of RA.

Conclusion

In conclusion, our study revealed that RA effectively preserved lung function in BLM-induced mice, reduced interstitial inflammation, and exerted an antifibrotic effect by reversing the downregulation of FGF1, Kit, Kras, and SRC in mouse lung tissues. Our findings provide novel evidence that BLM-induced PF in mice can be

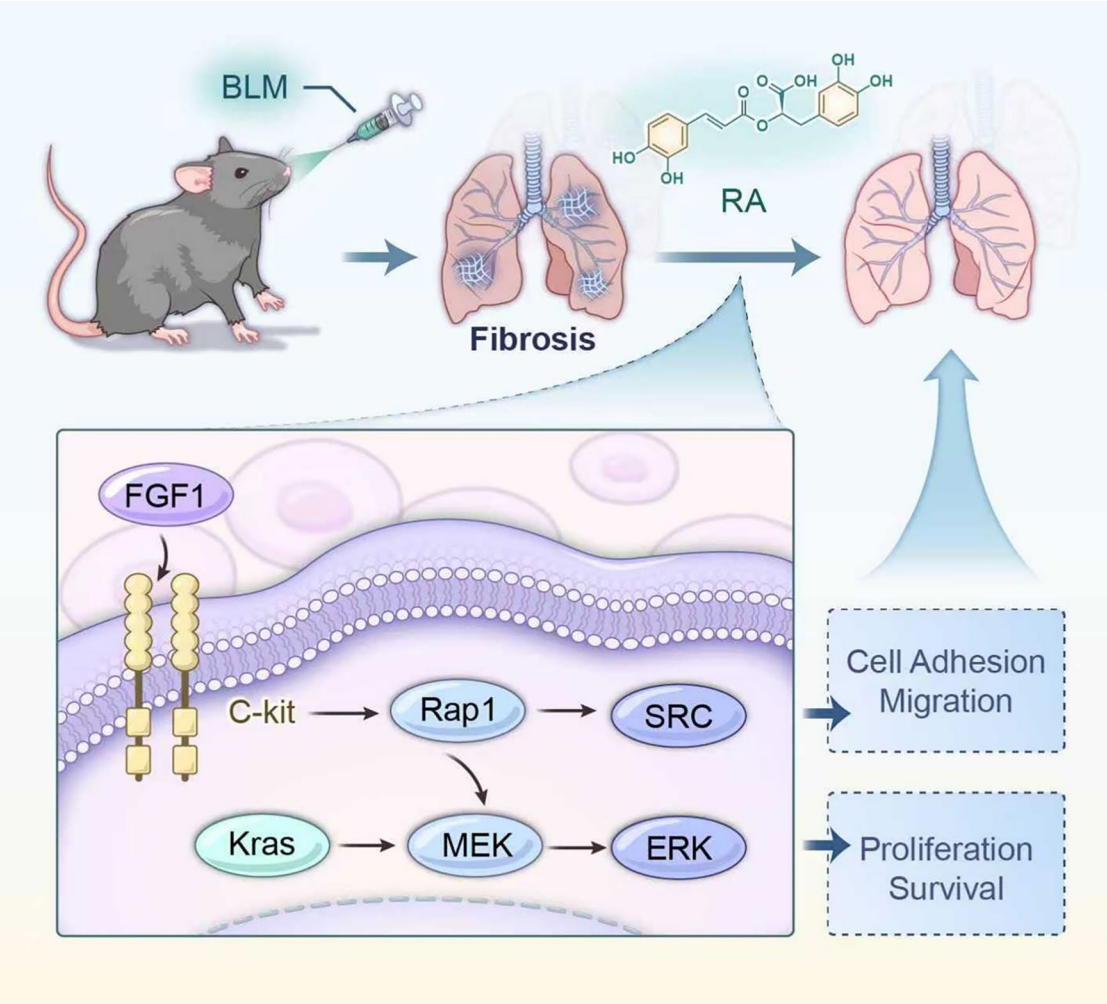

Fig. 10. The potential mechanism of RA in treating pulmonary fibrosis in mice. In the mice model of pulmonary fibrosis induced by bleomycin, RA showed an excellent therapeutic effect. In our research, we found that RA directly acts on proteins FGF1, c-KIT, SRC, and Kras. These proteins take the RAP1 signaling pathway as the keypoint to participate in downstream signaling pathways, to regulate cell proliferation, adhesion, metastasis, survival, and so on. Finally, RA can alleviate pulmonary fibrosis.

treated by RA through the RAP1 signaling pathway. The present results strongly suggest that RA may be a potential therapeutic remedy for PF.

Data availability

The datasets used and analyzed during the study are available from the corresponding authors on reasonable request.

Received: 3 November 2025; Accepted: 19 March 2026
Published online: 25 March 2026

References

1. Dinh, P. C. et al. Inhalation of lung spheroid cell secretome and exosomes promotes lung repair in pulmonary fibrosis. *Nat. Commun.* **11** (1), 1064 (2020).
2. Lederer, D. J. & Martinez, F. J. Idiopathic Pulmonary Fibrosis. *N. Engl. J. Med.* **378** (19), 1811–1823 (2018).
3. Hutchinson, J., Fogarty, A., Hubbard, R. & McKeever, T. Global incidence and mortality of idiopathic pulmonary fibrosis: a systematic review. *Eur. Respir. J.* **46** (3), 795–806 (2015).
4. Raghu, G. et al. Idiopathic pulmonary fibrosis in US Medicare beneficiaries aged 65 years and older: incidence, prevalence, and survival, 2001-11. *Lancet Respir. Med.* **2** (7), 566–572 (2014).
5. Esposito, D. B. et al. Idiopathic pulmonary fibrosis in United states automated claims: incidence, prevalence, and algorithm validation. *Am. J. Respir. Crit Care Med.* **192** (10), 1200–1207 (2015).
6. Raghu, G., Chen, S. Y., Hou, Q., Yeh, W. S. & Collard, H. R. Incidence and prevalence of idiopathic pulmonary fibrosis in US adults 18–64 years old. *Eur. Respir. J.* **48** (1), 179–186 (2016).

7. Allen, R. J. et al. Longitudinal lung function and gas transfer in individuals with idiopathic pulmonary fibrosis: a genome-wide association study. *Lancet Respir. Med.* **11** (1), 65–73 (2022).
8. Weill, D. et al. A consensus document for the selection of lung transplant candidates: 2014-an update from the Pulmonary Transplantation Council of the International Society for Heart and Lung Transplantation. *J. Heart Lung Transplant.* **34** (1), 1–15 (2015).
9. Raghu, G. et al. An Official ATS/ERS/JRS/ALAT clinical practice guideline: Treatment of idiopathic pulmonary fibrosis—an update of the 2011 clinical practice guideline. *Am. J. Respir. Crit Care Med.* **192** (2), e3–19 (2015).
10. King, T. E. Jr. et al. A phase 3 trial of pirfenidone in patients with idiopathic pulmonary fibrosis. *N. Engl. J. Med.* **370** (22), 2083–2092 (2014).
11. Richeldi, L. et al. Efficacy and safety of nintedanib in idiopathic pulmonary fibrosis. *N. Engl. J. Med.* **370** (22), 2071–2082 (2014).
12. Hua, Q. et al. PPARγ mediates the anti-pulmonary fibrosis effect of icaritin. *Toxicol. Lett.* **350**, 81–90 (2021).
13. Zhang, G. et al. Barbaloin attenuates pulmonary fibrosis through TGF-β1/Smads/p38 pathway. *J. Pharm. Pharmacol.* **74** (8), 1160–1169 (2022).
14. Zhao, Y. L. et al. Pharmacological effects of indole alkaloids from *Alstonia scholaris* (L.) R. Br. on pulmonary fibrosis in vivo. *J. Ethnopharmacol.* **267**, 113506 (2021).
15. Bing, P., Zhou, W. & Tan, S. Study on the mechanism of astragalus polysaccharide in treating pulmonary fibrosis based on drug-target-pathway network. *Front. Pharmacol.* **13**, 865065 (2022).
16. Guan, Z. et al. Isoandrographolide from Andrographis paniculata ameliorates tubulointerstitial fibrosis in ureteral obstruction-induced mice, associated with negatively regulating AKT/GSK-3β/β-cat signaling pathway. *Int. Immunopharmacol.* **112**, 109201 (2022).
17. Chavda, V. P. et al. The potential role of essential oils in boosting immunity and easing COVID-19 symptoms. *Clin. Tradit. Med. Pharmacol.* **5** (1), 200135 (2024).
18. Stafiniak, M. et al. Seasonal variations of rosmarinic acid and its glucoside and expression of genes related to their biosynthesis in two medicinal and aromatic species of salvia subg. *Perovskia Biol.-Basel.* **10** (6), 458 (2021).
19. Perra, M. et al. Formulation and testing of antioxidant and protective effect of hyalurosomes loading extract rich in rosmarinic acid biotechnologically produced from *Lavandula angustifolia* Miller. *Molecules* **27** (8), 2423 (2022).
20. Osakabe, N. et al. Anti-inflammatory and anti-allergic effect of rosmarinic acid (RA); inhibition of seasonal allergic rhinoconjunctivitis (SAR) and its mechanism. *Biofactors* **21** (1–4), 127–131 (2004).
21. Takano, H. et al. Extract of *Perilla frutescens* enriched for rosmarinic acid, a polyphenolic phytochemical, inhibits seasonal allergic rhinoconjunctivitis in humans. *Exp. Biol. Med.* **229** (3), 247–254 (2004).
22. Baba, S. et al. Absorption, metabolism, degradation and urinary excretion of rosmarinic acid after intake of *Perilla frutescens* extract in humans. *Eur. J. Nutr.* **44** (1), 1–9 (2005).
23. Ranjbar, A. et al. Antioxidant activity of Iranian *Echium amoenum* Fisch & C.A. Mey flower decoction in humans: A cross-sectional before/after clinical trial. *Evid.-Based Complement. Altern. Med.* **3** (4), 469–473 (2006).
24. Lee, J., Jung, E., Koh, J., Kim, Y. S. & Park, D. Effect of rosmarinic acid on atopic dermatitis. *J. Dermatol.* **35** (12), 768–771 (2008).
25. Connelly, A. E. et al. High-rosmarinic acid spearmint tea in the management of knee osteoarthritis symptoms. *J. Med. Food.* **17** (12), 1361–1367 (2014).
26. Noguchi-Shinohara, M. et al. Pharmacokinetics, safety and tolerability of *Melissa officinalis* extract which contained rosmarinic acid in healthy individuals: A randomized controlled trial. *PLoS One*. **10** (5), e0126422 (2015).
27. Lasrado, J. A. et al. Safety and tolerability of a dried aqueous spearmint extract. *Regul. Toxicol. Pharmacol.* **86**, 167–176 (2017).
28. Babaei, M. et al. Metabolic engineering of *Saccharomyces cerevisiae* for rosmarinic acid production. *ACS Synth. Biol.* **9** (8), 1978–1988 (2020).
29. Bahri, S. et al. Industrial elimination of essential oils from *Rosmarinus officinalis*: In support of the synergic antifibrotic effect of rosmarinic and carnosic acids in bleomycin model of lung fibrosis. *Nutr. Cancer*. **73** (11–12), 2376–2387 (2021).
30. Park, S. U., Uddin, R., Xu, H., Kim, Y. K. & Lee, S. Y. Biotechnological applications for rosmarinic acid production in plant. *Afr. J. Biotechnol.* **7**, 25 (2008).
31. Zhang, X. et al. Rosmarinic acid attenuates cardiac fibrosis following long-term pressure overload via AMPKα/Smad3 signaling. *Cell Death Dis.* **9** (2), 102 (2018).
32. Miao, C. G. et al. Wnt signaling in liver fibrosis: progress, challenges and potential directions. *Biochimie* **95** (12), 2326–2335 (2013).
33. Hsieh, Y. H., Tsai, J. P., Ting, Y. H., Hung, T. W. & Chao, W. W. Rosmarinic acid ameliorates renal interstitial fibrosis by inhibiting the phosphorylated-AKT mediated epithelial-mesenchymal transition in vitro and in vivo. *Food Funct.* **13** (8), 4641–4652 (2022).
34. Chen, Y. Y. et al. Anti-fibrotic effect of rosmarinic acid on inhibition of pterygium epithelial cells. *Int. J. Ophthalmol.* **11** (2), 189–195 (2018).
35. Zhang, T. et al. Rosmarinic acid prevents radiation-induced pulmonary fibrosis through attenuation of ROS/MYPT1/TGFβ1 signaling via miR-19b-3p. *Dose Response*. **18** (4), 1559325820968413 (2020).
36. Luo, Q. L. et al. Pharmacological investigation of a HPLC/MS standardized three herbal extracts containing formulae (Bu-Shen-Yi-Qi-Tang) on airway inflammation and hypothalamic-pituitary-adrenal axis activity in asthmatic mice. *Phytomedicine* **21** (11), 1439–1450 (2014).
37. Dickerhoff, J., Warnecke, K. R., Wang, K., Deng, N. & Yang, D. Evaluating molecular docking software for small molecule binding to G-Quadruplex DNA. *Int. J. Mol. Sci.* **22**, 19 (2021).
38. Gaillard, T. Evaluation of AutoDock and AutoDock Vina on the CASF-2013 benchmark. *J. Chem. Inf. Model.* **58** (8), 1697–1706 (2018).
39. Seeliger, D. & de Groot, B. L. Ligand docking and binding site analysis with PyMOL and Autodock/Vina. *J. Comput. Aided Mol. Des.* **24** (5), 417–422 (2010).
40. Kanehisa, M., Furumichi, M., Sato, Y., Matsuura, Y. & Ishiguro-Watanabe, M. KEGG: biological systems database as a model of the real world. *Nucleic Acids Res.* **53** (D1), D672–D677 (2025).
41. American Thoracic Society/European Respiratory Society International Multidisciplinary Consensus Classification of the Idiopathic Interstitial Pneumonias. This joint statement of the American Thoracic Society (ATS), and the European Respiratory Society (ERS) was adopted by the ATS board of directors, June 2001 and by the ERS Executive Committee, June 2001. *Am. J. Respir. Crit Care Med.* **165** (2), 277–304 (2002).
42. Umezawa, H., Suhara, Y., Takita, T. & Maeda, K. Purification of bleomycins. *J. Antibiot.* **19** (5), 210–215 (1966).
43. Walters, D. M. & Kleeberger, S. R. Mouse models of bleomycin-induced pulmonary fibrosis. *Curr. Protocols Pharmacol.* **5**, 46 (2008).
44. Henderson, N. C., Rieder, F. & Wynn, T. A. Fibrosis: from mechanisms to medicines. *Nature* **587** (7835), 555–566 (2020).
45. Itoh, N. & Ornitz, D. M. Fibroblast growth factors: from molecular evolution to roles in development, metabolism and disease. *J. BioChem.* **149** (2), 121–130 (2011).
46. Louzier, V. et al. Adenovirus-mediated fibroblast growth factor 1 expression in the lung induces epithelial cell proliferation: consequences to hyperoxic lung injury in rats. *Hum. Gene Ther.* **15** (8), 793–804 (2004).
47. Ramos, C. et al. Acidic fibroblast growth factor decreases alpha-smooth muscle actin expression and induces apoptosis in human normal lung fibroblasts. *Am. J. Physiol.-Lung Cell. Mol. Physiol.* **291** (5), L871–879 (2006).
48. Selman, M. & Pardo, A. Idiopathic pulmonary fibrosis: an epithelial/fibroblastic cross-talk disorder. *Respir. Res.* **3** (1), 3 (2002).

49. Selman, M. & Pardo, A. Alveolar epithelial cell disintegrity and subsequent activation: a key process in pulmonary fibrosis. *Am. J. Respir. Crit Care Med.* **186** (2), 119–121 (2012).
50. Selman, M. & Pardo, A. Revealing the pathogenic and aging-related mechanisms of the enigmatic idiopathic pulmonary fibrosis. an integral model. *Am. J. Respir. Crit Care Med.* **189** (10), 1161–1172 (2014).
51. Xu, X., Dai, H. & Wang, C. Epithelium-dependent profibrotic milieu in the pathogenesis of idiopathic pulmonary fibrosis: current status and future directions. *Clin. Respir. J.* **10** (2), 133–141 (2016).
52. Shimbori, C. et al. Fibroblast growth factor-1 attenuates TGF-β1-induced lung fibrosis. *J. Pathol.* **240** (2), 197–210 (2016).
53. Abbastabar, M. et al. Expression status of Rap1 pathway-related genes in liver metastases compared with corresponding primary colorectal cancer. *Cancers* **16** (1), 171 (2023).
54. Williams, D. E. et al. Identification of a ligand for the c-kit protooncogene. *Cell* **63** (1), 167–174 (1990).
55. Heinrich, M. C. et al. Correlation of long-term results of imatinib in advanced gastrointestinal stromal tumors with next-generation sequencing results: Analysis of phase 3 SWOG intergroup trial S0033. *Jama Oncol.* **3** (7), 944–952 (2017).
56. Goodman, V. L. et al. Approval summary: sunitinib for the treatment of imatinib refractory or intolerant gastrointestinal stromal tumors and advanced renal cell carcinoma. *Clin. Cancer Res.* **13** (5), 1367–1373 (2007).
57. Kelly, C. M., Gutierrez Sainz, L. & Chi, P. The management of metastatic GIST: current standard and investigational therapeutics. *J. Hematol. Oncol.* **14** (1), 2 (2021).
58. Blay, J. Y. et al. Ripretinib in patients with advanced gastrointestinal stromal tumours (INVICTUS): a double-blind, randomised, placebo-controlled, phase 3 trial. *Lancet Oncol.* **21** (7), 923–934 (2020).
59. Heinrich, M. C. et al. Avapritinib in advanced PDGFRA D842V-mutant gastrointestinal stromal tumour (NAVIGATOR): a multicentre, open-label, phase 1 trial. *Lancet Oncol.* **21** (7), 935–946 (2020).
60. Daniels, C. E. et al. Imatinib treatment for idiopathic pulmonary fibrosis: Randomized placebo-controlled trial results. *Am. J. Respir. Crit Care Med.* **181** (6), 604–610 (2010).
61. Hackett, T. L. et al. Characterization of side population cells from human airway epithelium. *Stem Cells*. **26** (10), 2576–2585 (2008).
62. Rock, J. R., Randell, S. H. & Hogan, B. L. Airway basal stem cells: a perspective on their roles in epithelial homeostasis and remodeling. *Dis. Models Mech.* **3** (9–10), 545–556 (2010).
63. Hoffman, A. M. et al. Lung-derived mesenchymal stromal cell post-transplantation survival, persistence, paracrine expression, and repair of elastase-injured lung. *Stem. Cells. Dev.* **20** (10), 1779–1792 (2011).
64. Reynolds, S. D. & Malkinson, A. M. Clara cell: progenitor for the bronchiolar epithelium. *Int. J. Biochem. Cell Biol.* **42** (1), 1–4 (2010).
65. Barkauskas, C. E. et al. Type 2 alveolar cells are stem cells in adult lung. *J. Clin. Invest.* **123** (7), 3025–3036 (2013).
66. Liu, Q. et al. c-kit(+) cells adopt vascular endothelial but not epithelial cell fates during lung maintenance and repair. *Nat. Med.* **21** (8), 866–868 (2015).
67. Suzuki, T. et al. c-Kit immunoexpression delineates a putative endothelial progenitor cell population in developing human lungs. *Am. J. Physiology-Lung Cell. Mol. Physiol.* **306** (9), L855–865 (2014).
68. Shi, W., Bellusci, S. & Warburton, D. Lung development and adult lung diseases. *Chest* **132** (2), 651–656 (2007).
69. Kolb, P. et al. The importance of interventional timing in the bleomycin model of pulmonary fibrosis. *Eur. Respir. J.* **55**(6) (2020).
70. Sheikh, E., Tran, T., Vranic, S., Levy, A. & Bonfil, R. D. Role and significance of c-KIT receptor tyrosine kinase in cancer: A review. *Bosnian J. Basic. Med. Sci.* **22** (5), 683–698 (2022).
71. Poźniak, M. et al. The significance of cell surface N-glycosylation for internalization and potency of cytotoxic conjugates targeting receptor tyrosine kinases. *Int. J. Mol. Sci.* **23** (15), 8514 (2022).
72. Parikh, K. et al. Drugging KRAS: current perspectives and state-of-art review. *J. Hematol. Oncol.* **15** (1), 152 (2022).
73. Ryan, D. P., Hong, T. S. & Bardeesy, N. Pancreatic adenocarcinoma. *N. Engl. J. Med.* **371** (11), 1039–1049 (2014).
74. Forbes, S. A. et al. COSMIC: exploring the world's knowledge of somatic mutations in human cancer. *Nucleic Acids Res.* **43** (D1), D805–811 (2015).
75. Leevers, S. J., Paterson, H. F. & Marshall, C. J. Requirement for Ras in Raf activation is overcome by targeting Raf to the plasma membrane. *Nature* **369** (6479), 411–414 (1994).
76. Ferro, E. & Trabalzini, L. RalGDS family members couple Ras to Ral signalling and that's not all. *Cell. Signal.* **22** (12), 1804–1810 (2010).
77. Castellano, E. & Downward, J. RAS Interaction with PI3K: More than just another effector pathway. *Genes Cancer*. **2** (3), 261–274 (2011).
78. Simanshu, D. K., Nissley, D. V. & McCormick, F. RAS proteins and their regulators in human disease. *Cell* **170** (1), 17–33 (2017).
79. Ogawa, F. et al. Role of KRAS in regulating normal human airway basal cell differentiation. *Respir. Res.* **20** (1), 181 (2019).
80. Feng, J. et al. Targeting metabolic vulnerability in mitochondria conquers MEK inhibitor resistance in KRAS-mutant lung cancer. *Acta Pharm. Sinica B*. **13** (3), 1145–1163 (2023).
81. Lv, W., Wu, Y. & Chen, H. Orthogonal upconversion nanocarriers for combined photodynamic therapy and precisely triggered gene silencing in combating keloids. *J. Controlled Release*. **379**, 1–13 (2025).
82. Roskoski, R. Jr. Src kinase regulation by phosphorylation and dephosphorylation. *Biochem. Biophys. Res. Commun.* **331** (1), 1–14 (2005).
83. Gao, J. et al. Buyang Huanwu decoction ameliorates myocardial injury and attenuates platelet activation by regulating the PI3 kinase/Rap1/integrin α(IIb)β(3) pathway. *Chin. Med.* **19** (1), 109 (2024).
84. Ishizawar, R. & Parsons, S. J. c-Src and cooperating partners in human cancer. *Cancer Cell.* **6** (3), 209–214 (2004).
85. Hanna, Z. et al. The pathogenicity of human immunodeficiency virus (HIV) type 1 Nef in CD4C/HIV transgenic mice is abolished by mutation of its SH3-binding domain, and disease development is delayed in the absence of Hck. *J. Virol.* **75** (19), 9378–9392 (2001).
86. Chin, J. et al. Fyn kinase induces synaptic and cognitive impairments in a transgenic mouse model of Alzheimer's disease. *J. Neurosci.* **25** (42), 9694–9703 (2005).
87. Kojima, N., Ishibashi, H., Obata, K. & Kandel, E. R. Higher seizure susceptibility and enhanced tyrosine phosphorylation of N-methyl-D-aspartate receptor subunit 2B in fyn transgenic mice. *Learn. Mem.* **5** (6), 429–445 (1998).
88. Beyer, C. & Distler, J. H. Tyrosine kinase signaling in fibrotic disorders: Translation of basic research to human disease. *Biochim. Biophys. Acta*. **1832** (7), 897–904 (2013).
89. Abdalla, M. et al. Dasatinib inhibits TGFβ-induced myofibroblast differentiation through Src-SRF Pathway. *Eur. J. Pharmacol.* **769**, 134–142 (2015).
90. Wang, G. et al. The Anti-fibrosis drug Pirfenidone modifies the immunosuppressive tumor microenvironment and prevents the progression of renal cell carcinoma by inhibiting tumor autocrine TGF-β. *Cancer Biol. Ther.* **23** (1), 150–162 (2022).
91. Zeng, X. et al. Mechanism-guided drug development and treatment for liver fibrosis: a clinical perspective. *Front. Pharmacol.* **16**, 1574385 (2025).

Acknowledgements

We are very appreciating those valuable discussions from Dr. Huang Qi from Shanghai Gamma Hospital. We thank Shanghai Applied Protein Technology Co. for the help with proteomics analysis. We are grateful to Kanehisa laboratories for authorizing us to use KEGG pathway data in the manuscript.

Author contributions

Aman GUL, Yuanyuan Zhong: Conceptualization, Methodology, Investigation, Validation, Writing-Original Draft. Maimaiti AILI, Cong XIE: Methodology, Resources. Ainiwaer Talifu, Shixia HUO: Formal analysis, Investigation. Yilifanjiang KUERBAN, Maimaititusun Yalkun: Methodology, Investigation. Jingcheng Dong, Zhi Jian Li: Supervision, Writing - Review & Editing. All the authors have read and approved the final version of the manuscript.

Funding

This research was funded by the Special Project for Young Science and Technology Talents of the Administration of Traditional Chinese Medicine of Xinjiang Uygur Autonomous Region, grant nmuber "No.ZYQ2025018", the Scientific Research and Technological Development Program of the Science and Technology Bureau of Tianshan District, grant number "WLMQTSQ-2025-KJXM04", and the National Natural Science Foundation regional project, grant number "82460871".

Declarations

Competing interests

The authors declare no competing interests.

Ethics approval

All animals were handled in strict accordance with the relevant national and local animal wel-fare bodies, and all experiments were approved by the Experimental Animal Ethics Committee of Fudan University (permit number: 2020-12-HSYY-DJC-01) and the Experimental Animal Eth-ics Committee of Xinjiang Medical University (permit number: IACUC-20240226-06).

Additional information

Supplementary Information The online version contains supplementary material available at https://doi.org/10.1038/s41598-026-45457-6.

Correspondence and requests for materials should be addressed to Z.J.L. or J.D.